CYBERNETICS AND PHYSICS, VOL. 3, NO. 3, 2014 , 130–136

ADVANCED SIMULATION TOOLS FOR MUON-BASED ACCELERATORS

Pavel Snopok
Physics Department
Illinois Institute of Technology
USA
psnopok@iit.edu

James Ellison
Physics Department
Illinois Institute of Technology
USA
jelliso1@hawk.iit.edu

Josiah Kunz
Physics Department
Illinois Institute of Technology
USA
jkunz@hawk.iit.edu

Abstract

High Energy Physics relies on particle accelerators of the highest energy to discover and elucidate the fundamental forces of nature. Electron-positron colliders are limited in center-of-mass energy because of radiative processes. Proton colliders, because of the composite nature of the proton, must have even higher energy and will require enormous amounts of real estate. In contrast, a muon collider ring of up to 6 TeV center-of-mass energy has a radius of ≈ 1 km. New computational tools are essential for accurate modeling and simulation of the next generation of muon-based accelerator experiments at the energy and intensity frontiers. This article summarizes the current effort in development of new tools based on modern software frameworks and incorporating the most accurate theoretical calculations available. Crucial physics processes specific to muon accelerators are implemented in the set of modeling tools. These include such specialized processes as collective and plasma effects in matter, multiple scattering in high magnetic fields, and the influence of ionization-cooling absorbers on standard collective effects such as space charge and wake fields.

Key words

muon accelerator, modeling, simulation tools, matter-dominated lattices, ionization cooling, plasma effects

1 Introduction

A prime example of why muon accelerators are relevant comes from the prospect of a neutrino factory or a muon collider [Muon Accelerator Program]. As muon branching fractions are nearly 100% $\mu^- \to e^- \bar{\nu}_e \nu_\mu$ and $\mu^+ \to e^+ \nu_e \bar{\nu}_\mu$, there are obvious advantages of a muon-sourced neutrino beam. Also, due to the fact that muons are roughly 200 times heavier than electrons, synchrotron radiation is not an issue, and as a result a high-energy muon collider ($\sqrt{s} = 6$ TeV) could be built on a relatively compact site (where the collider ring is about 6 km in circumference). This energy level is experimentally unprecedented in the leptonic sector, since a circular electron accelerator would be restricted by vast amounts of synchrotron radiation. At lower energy, a muon collider could serve as a Higgs factory ($\sqrt{s} = 126$ GeV), with possible new physics via the observation of Higgs to lepton coupling. This is advantageous, since the Higgs theoretically couples more strongly to muons than electrons because of the small electron mass.

Muon-based facilities are not without their challenges. Synthetic muon creation comes from the collision of protons with a fixed target. The resultant spray of particles largely contains kaons (which decay primarily into pions and muons), pions (which decay primarily into muons), and rogue protons. High-intensity collection necessitates a large initial phase space volume. The resultant cloud of muons with momenta centered around 200-250 MeV$/c$ must be collected, focused, and accelerated well within the muon lifetime (2.2 μs at rest). Therefore, the slow beam cooling (beam size reduction) techniques used in proton and electron accelerators cannot be used. Due to the short-lived nature of the muon, novel beam cooling techniques have been explored and ionization cooling in particular has been shown to work well [Budker, 1970].

Along with ionization cooling, a number of other processes such as collective and plasma effects in matter, multiple scattering in high magnetic field, and the influence of ionization-cooling absorbers on standard collective effects such as space charge are considered important, and are being studied and implemented in the modeling codes described below.

2 Matter-Dominated Lattices

In the ionization cooling technique, muons traverse a certain amount of material in order to lose energy in both longitudinal and transverse directions due to ionization. The energy is then restored in the longitudinal direction only by passing through a set of RF cavities,

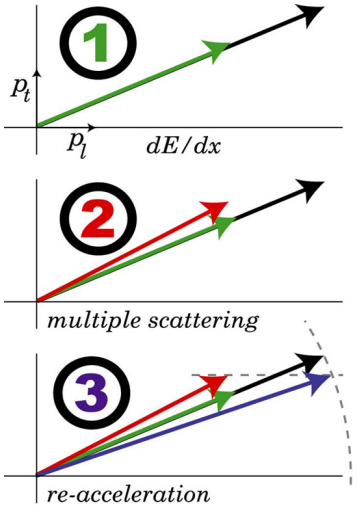

Figure 1. Vector representation of ionization cooling. 1) Energy loss in material, both transverse and longitudinal momenta are reduced. 2) Increase in the transverse momentum due to multiple scattering. 3) Re-acceleration through the RF cavity resulting in the net reduction in the transverse momentum.

leading to an overall reduction in the transverse direction (cooling). In vector form, this can be seen in Fig. 1, where this process is split into three parts.

The evolution of the normalized transverse emittance can be described by the following equation [Neuffer, 1983]:

$$\frac{d\epsilon_n}{dz} \approx -\frac{1}{\beta^2}\langle\frac{dE_\mu}{dz}\rangle\frac{\epsilon_n}{E_\mu} + \frac{1}{\beta^3}\frac{\beta_\perp E_s^2}{2E_\mu mc^2 X_0}, \qquad (1)$$

where ϵ_n is the normalized emittance, z is the path length, E_μ is the muon beam energy, $\beta = v/c$, X_0 is the radiation length of the absorber material, $\beta_\perp$ is the betatron function, and E_s is the characteristic scattering energy. Here, two competing effects can be seen: the first term is the cooling (reduction of phase space beam size) component from ionization energy loss and the second term is the heating (increase of phase space beam size) term from multiple scattering. This highlights the importance of the stochastic terms, as the only deterministic term is the expected (Bethe-Bloch) energy loss, $\langle\frac{dE_\mu}{dz}\rangle$.

3 Simulation Tools

There are two common types of general beam-physics simulation codes: single-particle codes that integrate the equations of motion for every single particle passing through the system, and transfer map codes that evaluate the overall effect of the lattice on the particles first by producing a transfer map, and then applying it to a given initial distribution of particles. Both types of established codes are improved and advanced. Specifically, for addressing muon accelerator modeling problems, the two codes under active development, G4beamline [G4beamline] and COSY Infinity [Berz, Makino, COSY Infinity] are selected.

G4beamline is chosen for its flexibility and modularity promoting development of new computational tools. In addition, G4beamline is one of the *de facto* standard codes used by the muon community. As such, it has implemented a large number of relevant processes already, so improvements will contribute immediately.

COSY was selected for its computational speed, ability to produce high-order transfer maps, and ability to control individual aberrations, which is essential for the large emittance beams under consideration. Further, at the language level COSY has the advantage of built-in optimization tools.

While these two codes are being actively improved, the other independent codes such as ICOOL [ICOOL] are used for benchmarking and verifying the results.

4 G4beamline

G4beamline is a single-particle-tracking simulation program optimized for beamlines, which is based on the Geant4 toolkit [Geant4]. G4beamline has a large library of common elements used in particle accelerators and detectors. Particles are tracked using the full accuracy of the Geant4 toolkit. To permit tradeoffs between accuracy and computation time, several different models for hadronic interactions as well as a large amount of experimental data are available for use by the more detailed models. The result is that G4beamline can provide a realistic assessment of how the system will behave. To assist the user in verifying that the simulated system accurately represents the real system, extensive visualization capabilities are included in G4beamline.

A number of processes such as energy-loss straggling model, energy loss in the matter for high-energy muons, collective and plasma effects in matter, multiple scattering in high magnetic field, and the influence of ionization-cooling absorbers on standard collective effects such as space charge are either missing or not implemented to the desired level of confidence in G4beamline. The list of these processes is being prioritized, and the most crucial processes are being implemented (or interfaced with G4beamline if they exist in other software packages).

4.1 Multiple Scattering in Strong Magnetic Field

The first process addressed is that of multiple scattering in the magnetic field. Extensive studies were performed to cover a range of materials and magnetic fields from 0 to 100 T in order to identify the effect and the size of the required physics step in the code that produced consistent results. This effect produced a dramatic change over the range of steps for different values of the magnetic field, as can be seen in Figure 2 (top). Generally, this effect is weaker for the relevant values of the magnetic field (0-30 T) if the physics step prescribed by the G4beamline command maxStep is set

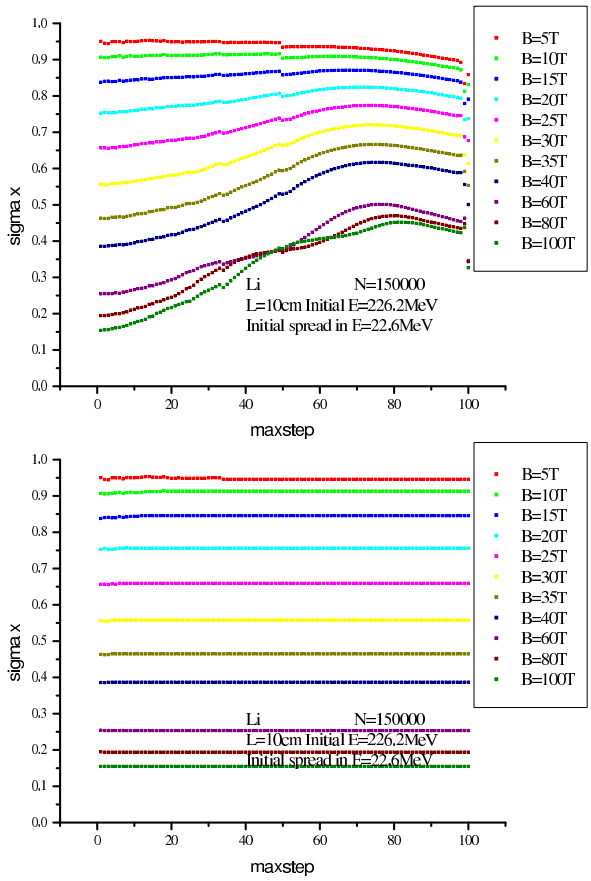

Figure 2. Top: Dependence of multiple scattering in material on step size (horizontal axis) and magnetic field (colors); bottom: the same simulation after an automatic step limiting algorithm is implemented, step is limited inside the material only.

to less than 1-5 mm depending on the strength of the field. Given the recent advances in code speed-up (35x on a single CPU), this choice of maxStep (step is limited inside the material only) is not expected to result in prohibitively slow simulations. It was found that the maximum step that should be allowed to be taken did not vary with material, only the strength of the field. A curve was then fitted to this minimum value versus the magnetic field. The maximum step that should be allowed was found to vary with field as

$$\text{maxStep} = \frac{100\text{ mm}}{10^{-2}B^2 + 0.35B + 1},$$

where B is the strength of the magnetic field in Tesla.

Based on the study outcomes, an algorithm automatically limiting the value of maxStep depending on the absorber material properties and the magnetic field strength was implemented in G4beamline and applied. The results are shown in Fig. 2 (bottom). Details of the simulation can be found in [Snopok *et al.*, 2013].

Associated with the first problem was the issue of the tail of the multiple scattering distribution in the presence of a strong magnetic field not being consistent between the Molière model and the discrete scattering approach producing a more trustworthy results, but too slow to be used for production runs [Lebrun, 1999]. A study was carried out recreating the problematic lattice, and it was concluded that the new scattering model based on the Lewis theory implemented in Geant4, which G4beamline is currently based upon, follows the tail of the discrete scattering distribution much more closely than the old Molìere model used in Geant3 [Geant3; Snopok *et al.*, 2013]. Hence, no further action was required in terms of improving the code. Figure 3 shows the beam spread at a certain point in the lattice for the different models used. The data points were obtained using a digital graph analyzer on the plots in [Lebrun, 1999].

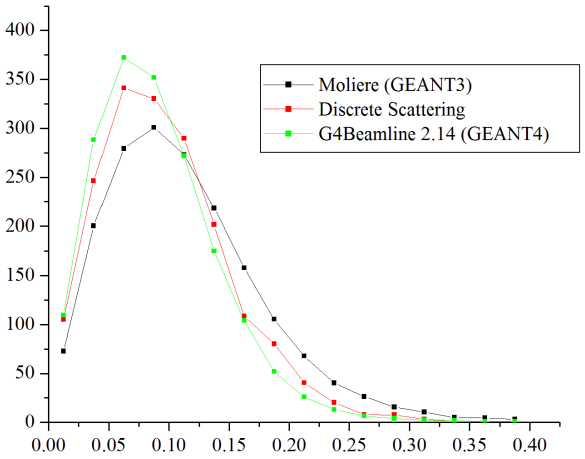

Figure 3. Comparison of the beam spread distribution for different models. Data for the Molière and discrete scattering models were taken from [Lebrun, 1999]. G4beamline simulation matches the tail of the discrete scattering distribution much better than the older Molière model.

4.2 Plasma Effects and Future Work

At present, there is a change of focus toward studying the ionization effects in the absorber matter caused by the muon beam passing through. Ionization changes material properties and that, in turn, affects the beam. These effects motivate further studies and detailed simulations. It was shown previously that plasma will not have an adverse effect on the beam [Ahmed *et al.*, 2012], but there was no detailed study of the potential changes in the beam cooling rate crucial for muon beam applications.

5 COSY Infinity

COSY Infinity [Berz, Makino, COSY Infinity] is an arbitrary-order beam dynamics simulation and analysis code. It allows the study of accelerator lattices, spectrographs, beamlines, electron microscopes, fragment separators, and other devices. It can determine high-order maps of combinations of particle optical elements of arbitrary field configurations. The elements can either be based on a large library of exist-

ing elements with realistic field configurations including fringe fields, or described in detail by measured data. COSY has its own programming language, and a differential algebra based computation engine. It includes built-in optimization at the language level. For precision modeling, design, and optimization of next-generation muon beam facilities, its features make it the ideal code. The main component that needs to be included in COSY is the algorithm necessary to follow the distribution of charged particles through matter.

Muons are tertiary production particles and high-intensity collection necessitates a large initial phase space volume. Therefore, accurate modeling of the dynamics and correction of aberrations is imperative. To study in detail some of the properties of particles passing through material, the transfer map approach alone is not sufficient. The interplay of beam optics and atomic processes must be studied by a hybrid transfer map-Monte-Carlo approach in which transfer map methods are used when there is no material in the accelerator channel, and Monte-Carlo methods when particles pass through material.

COSY is particularly advantageous to use when considering the efficient use of computational time. This is due to the transfer map methods that COSY employs. Given an initial phase space vector $\mathbf{Z_0}$ at s_0 that describes the relative position of a particle with respect to the reference particle, and assuming the future evolution of the system is uniquely determined by $\mathbf{Z_0}$, we can define a function called the transfer map relating the initial conditions at s_0 to the conditions at s via $\mathbf{Z}(s) = \mathbf{M}(s_0, s) \circ \mathbf{Z}(s_0)$. The transfer map formally summarizes the entire action of the system. The composition of two maps yields another map: $\mathbf{M}(s_0, s_1) \circ \mathbf{M}(s_1, s_2) = \mathbf{M}(s_0, s_2)$, which means that transfer maps of systems can be built up from the transfer maps of the pieces. Computationally this is advantageous because, once calculated, it is much faster to apply a single transfer map to a distribution of particles than to track individual particles through multiple lattice elements.

Currently supported elements in COSY include various magnetic and electric multipoles (with fringe effects), homogeneous and inhomogeneous bending elements, Wien filters, wigglers and undulators, cavities, cylindrical electromagnetic lenses, general particle optical elements, and *deterministic* absorbers of intricate shapes described by polynomials of arbitrary order, with the last element being of particular interest for this study. The term deterministic is deliberately emphasized, since the polynomial absorber acts like a drift with the average (Bethe-Bloch) energy loss. The advantage of this is that the user must only specify six material parameters in order for COSY to calculate this energy loss: the atomic number, atomic mass, density, ionization potential, and two correction parameters.

However, this element only takes into account deterministic effects (producing the same final result every time for the same initial condition), not stochastic effects (intrinsically random effects such as multiple scattering and energy straggling). For a realistic simulation of a beam of particles through matter, one needs to take into account both the former and the latter, according to Eq. (1).

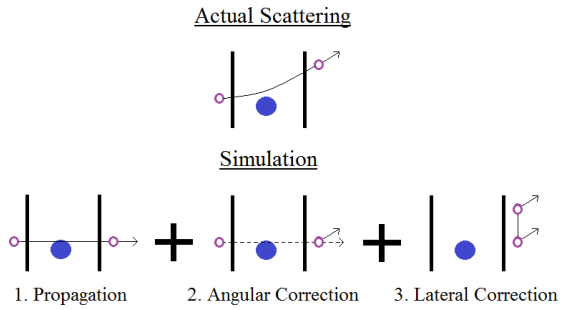

Figure 4. Top: a depiction of classical scattering; bottom: an algorithm producing a similar effect.

It is clear why stochastic effects do not fit well into the transfer map paradigm: two identical particles with identical initial coordinates will follow two different paths inside the absorber material (due to the intrinsically random nature of multiple scattering). Therefore, it is not possible to construct a traditional transfer map that represents the absorber, as this would require uniquely relating the coordinates after the absorber to the coordinates before the absorber. In light of this, the effort of integrating stochastic processes into COSY focuses on particle-by-particle propagation (as opposed to transfer map methods). Furthermore, in the spirit of efficiency, this integration should endeavor to greatly increase the step size of such algorithms, and to include other possible improvements.

The typical treatment of multiple scattering involves three steps: free propagation, angular correction, and lateral displacement correction, as depicted by Figure 4. As previously discussed, Fig. 4 shows only one of many possibilities. The angular correction and lateral displacement are chosen from probability distributions, which vary by material, absorber length, and initial energy. Figure 5 clearly shows the dependence of the lateral correction on absorber length corresponding to longitudinal momentum losses of 5, 10, 15, and 20 MeV$/c$. Since the initial distribution is a pencil beam (i.e. $x = p_x = \sigma_x = \sigma_{p_x} = 0$), Figure 5 shows virtually all of the different possible final states for 10^4 muons with the same initial conditions. From here the probability distribution of the lateral displacement correction can be ascertained as roughly Gaussian, where the Gaussian mean is always zero (i.e. the most probable scenario is no net scattering) and the Gaussian σ appears to be some function of absorber length, and possibly absorber material and initial energy. More precisely, the distribution should follow Goudsmit-Saunderson theory [Goudsmit and Saunderson, 1940] for small angles and have a Rutherford distribution for large angles. Then the (unnormalized) dis-

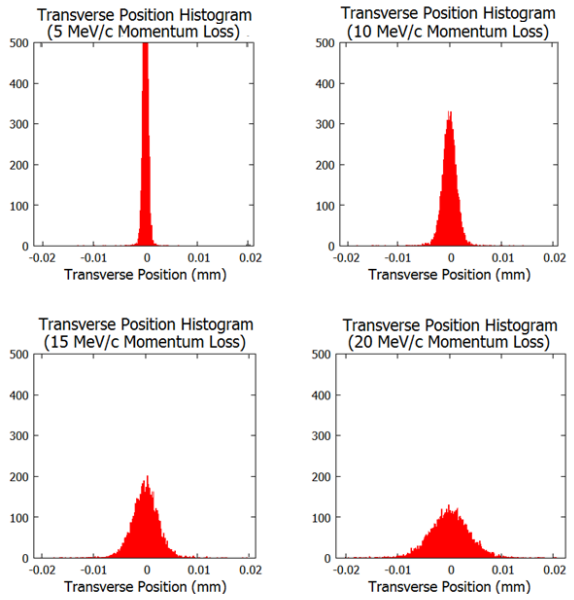

Figure 5. 10^4 muons were simulated with ICOOL [ICOOL] through various lengths of liquid hydrogen. These transverse position histograms were obtained from a pencil beam with an initial momentum of precisely 200 MeV$/c$.

tribution that represents the angular correction can be described by Eq. (2), which takes into account continuity and smoothness:

$$g(u) = \begin{cases} e^{-a(1-u)}, & u_0 \le u \quad (P_x \le P_{x_0}) \\ \dfrac{4e^{-3}}{(a-1-au)^2}, & u \le u_0 \quad (P_{x_0} \le P_x) \end{cases}, \tag{2}$$

where $u = \cos\theta = P_z/\sqrt{P_z^2 + P_x^2}$, $u_0 = 1 - 3/a$, and $P_{x_0} = P_z\sqrt{(\frac{a}{a-3})^2 - 1}$. Here the Gaussian profile mentioned earlier is recovered for small P_x, as $1/\sqrt{1 + (P_x/P_z)^2} \approx 1 - 0.5(P_x/P_z)^2$.

The scattering profile is now in terms of the variable a. According to modified Highland-Lynch-Dahl theory, it is possible to write:

$$a(L, E_i) = \frac{0.5}{1 - \cos(\theta_0(L, E_i))},$$

where

$$\theta_0(L, E_i) = \frac{13.6\ \text{MeV}}{\beta cp} z_{ch} \left[\frac{t}{X_0}\right]^{0.555}$$

has been slightly modified [Lynch and Dahl, 1975]. Here, $\beta = v/c$, p is the total initial momentum, z_{ch} is the charge of the incident particle, t is the so-called "true path length" (here approximated simply as the step size), and X_0 is the radiation length of the material. Finally, it is possible to explicitly see the dependence of the scattering distribution on the absorber material (X_0), absorber length (t), and initial energy (βcp).

In a similar fashion, straggling (fluctuation about a mean energy loss) may be simulated. The energy loss profile follows a Landau distribution of the form [Landau, 1944]:

$$f(\lambda) = \frac{1}{\xi}\frac{1}{2\pi i}\int_{c-i\infty}^{c+i\infty} \exp(u\ln u + \lambda u)du, \tag{3}$$

where $c \ge 0$ and

$$\lambda = (\varepsilon - \bar{\varepsilon})/\xi - \gamma' - \beta^2 - \ln(\xi/E_{\max}),$$

ε is the energy loss variable, $\bar{\varepsilon}$ is the average energy loss (which is already calculated by baseline COSY), $\gamma' = 0.422784\ldots = 1 - \gamma_{\text{Euler}}$, and $E_{\max}$ and ξ are defined as

$$\begin{aligned} E_{\max} &= \frac{2m_e\beta^2\gamma^2}{1 + 2\gamma m_e/m_x + (m_e/m_x)^2}, \\ \xi &= \frac{2\pi z_{ch}^2 e^4 N_A Z\rho}{Am_e c^2}\frac{L}{1 - m_x^2/E_i^2}. \end{aligned} \tag{4}$$

Here, m_e is the mass of the electron, $\gamma = 1/\sqrt{1-\beta^2}$, m_x is the mass of the incident particle, e is the fundamental charge, N_A is Avogadro's number, Z is the nucleic charge of the material, ρ is the material density, A is the atomic number of the material, L is the length of the absorber, and E_i is the incident energy of the particle.

For implementation reasons, it is more helpful to use the Landau function where the energy loss is parameterized as

$$\lambda = (\varepsilon - \alpha)/\beta_L,$$

where α is approximately the most probable value and β_L is a "scaling factor" referred to as the Landau beta. By comparison with the former parameterization, it is easy to infer that $\beta = \xi$ and that

$$\begin{aligned} \alpha(L, E_i) = \bar{\varepsilon} + \beta_L(L, E_i)\times \\ \times \left[2 - \gamma_{\text{Euler}} - \frac{m_x^2}{E_i^2} + \ln\left(\frac{\beta_L(L, E_i)}{E_{\max}}\right)\right]. \end{aligned}$$

Equations (2)–(4) (with the variables a, β_L, and α as functions of material, absorber length, and initial energy) were implemented into COSY as post-absorber corrections. Figures 6 and 7 show the results of these implementations compared to ICOOL [ICOOL] and G4Beamline, where ICOOL uses Vavilov straggling and Bethe-modified Molière scattering. The initial beam parameters for this simulation were 5×10^4

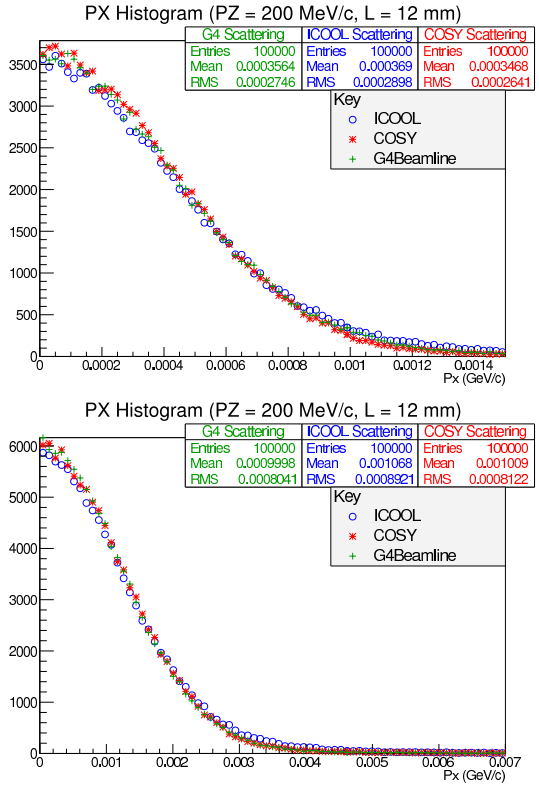

Figure 6. $|P_x|$ histogram comparison between COSY Infinity, ICOOL, and G4Beamline showing good agreement between the codes. Top plot is liquid hydrogen, bottom plot is lithium hydride.

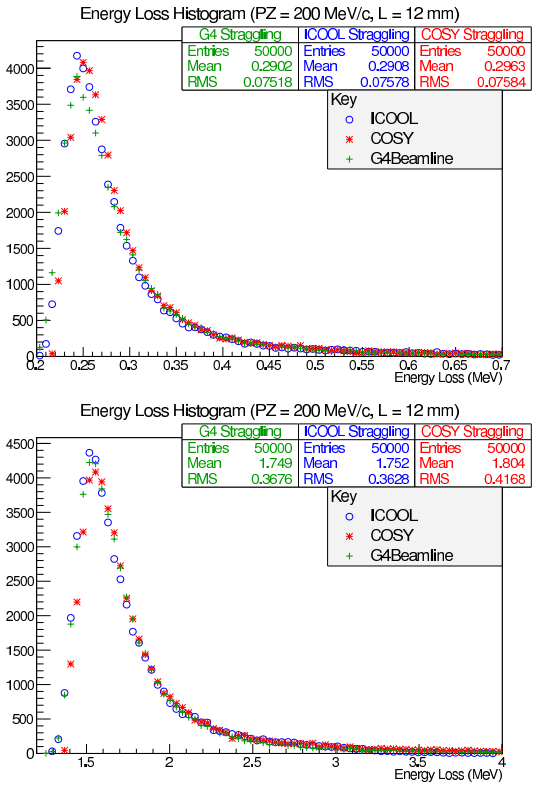

Figure 7. Energy loss histogram comparison between COSY Infinity, ICOOL, and G4Beamline showing good agreement between the codes. Top plot is liquid hydrogen, bottom plot is lithium hydride.

muons through 12 mm of liquid hydrogen (top) and lithium hydride (bottom) with $(x, \sigma_x, P_x, \sigma_{P_x}, \sigma_{P_z}) = \overrightarrow{0}$ (pencil beam), where x signifies the arbitrary transverse direction, and $P_z = 200$ MeV/c.

Based on the current results, future work should include several improvements. The most obvious improvement is to increase the step size even further: up to, for example, 10 cm. For scattering, it is presently unclear how this increase will affect the theoretical curves. On the other hand, when considering energy loss effects theory predicts a Vavilov distribution of the form [Vavilov, 1957]:

$$f(\varepsilon) = \frac{1}{\xi}\varphi_v(\lambda_v, \kappa, \beta^2),$$

where

$$\varphi_v(\lambda_v, \kappa, \beta^2) = \frac{1}{2\pi i}\int_{c-i\infty}^{c+i\infty} \exp[\kappa(1+\beta^2\gamma) + \psi(s) + \lambda s]ds, c \geq 0,$$

$$\psi(s) = s\ln\kappa + (s+\beta^2\kappa)\left[\ln(s/\kappa) + E_1(s/\kappa)\right] - \kappa e^{-s/\kappa},$$

$$E_1(z) = \int_{\infty}^{z} t^{-1}e^{-t}dt,$$

$$\kappa(L, E_i) = \xi/E_{\max}.$$

Recall that $E_{\max}$ and ξ can be found in Eq. (4). λ_v can be shown to be related to the Landau λ as $\lambda = \lambda_v/\kappa - \ln\kappa$. Moreover, as $\kappa \to 0$ the Vavilov distribution tends to the Landau distribution, and as $\kappa \to \infty$ the Vavilov distribution tends to a Gaussian distribution. For computational efficiency it is common to set these limits as

$$f(\varepsilon) = \begin{cases} \text{Landau}, & \kappa \leq 0.01 \\ \text{Vavilov}, & 0.01 \leq \kappa \leq 10 \\ \text{Gauss}, & 10 \leq \kappa \end{cases}.$$

5.1 Future Work

Further improvements to the code should include very small step sizes ($\sim$0.1 mm) for the purpose of propagation of the beam through absorbers inside of high magnetic fields. For any realistic simulation of muons, decay processes must be included as well. This naturally leads to the inclusion in the code of daughter particle tracking. Finally, the algorithms presented here should be subject to comparison with experimental results, such as the MuScat experiment [Attwood *et al.*, 2006].

6 Summary

Muon-based neutrino sources are enticing due to their ability to create consistent, high-intensity mixed neutrino beams. On the other hand, muon colliders present

an opportunity to conduct leptonic experiments at unprecedented energy levels while keeping the facility size quite compact. However, for any such facility ionization cooling is a crucial component. The design of these novel cooling channels requires many simulation software tools to be augmented with new experimental results for various types of absorbers. G4beamline and COSY Infinity have many features for advanced lattice design, and will in the future be outfitted with tools that help accurately evaluate matter-dominated lattices of a wide variety.

7 Acknowledgements

The authors would like to thank Prof. Martin Berz from Michigan State University and Dr. Thomas Roberts from Muons, Inc. for many fruitful discussions and their invaluable advice.

References

Ahmed, S., Kaplan, D., Roberts, T., Spentzouris, L., and Beard, K. (2012) Interaction of muon beam with plasma developed during ionization cooling. In: *Proc. IPAC 2012*, TUEPPB001, http://accelconf.web.cern.ch/AccelConf/IPAC2012/papers/tueppb001.pdf.

Attwood, D., et al. (2006) The scattering of muons in low-Z materials, *NIM B251,* p. 41.

Budker, G. I. (1970) In: *Proc. 15th Int. Conf. on High Energy Physics,* Kiev.

M. Berz, K. Makino, COSY Infinity, http://www.cosyinfinity.org.

G4beamline, http://www.muonsinternal.com/muons3/G4beamline.

Geant3 User Manual, http://wwwasdoc.web.cern.ch/wwwasdoc/pdfdir/geant.pdf.

Geant4 User Documentation, http://geant4.cern.ch/support/userdocuments.shtml.

Goudsmit, S., and Saunderson, J. L. (1940) Multiple scattering of electrons. *Phys. Rev. 57,* p. 24.

Fernow, R. C. et al., ICOOL Simulation Code, http://www.cap.bnl.gov/ICOOL/.

Landau, L. (1944) On the energy loss of fast particles by ionisation, *J. Phys 8,* p. 201.

Lebrun, P. (1999) MuCool Note #30, http://nfmcc-docdb.fnal.gov/cgi-bin/ShowDocument?docid=30 and MuCool Note #33, http://nfmcc-docdb.fnal.gov/cgi-bin/ShowDocument?docid=33.

Lynch, G. R., and Dahl, O. I. (1975) Approximations to multiple coulomb scattering, *NIM B58,* p. 6.

Muon Accelerator Program, http://map.fnal.gov.

Neuffer, D. (1983) Principles and Applications of Muon Cooling, *Part. Acc. 14,* p. 75.

Snopok, P., Ellison, J., and Roberts, T. (2013) Multiple scattering effects in a strong magnetic field. In: *Proc. PAC 2013,* MOPBA09, Pasadena.

Vavilov, P. V. (1957) Ionization losses of high-energy heavy particles, *J. Exptl. Theoret. Phys. (U.S.S.R.) 5,* p. 920.